8-BD

Gas Kick Behavior During Bullheading Operations

by

Principal Investigator: Adam T. Bourgoyne, Jr., Ph.D.
Associate Researchers: William L. Koederitz, Ph.D.
Petroleum Engineering Department
Louisiana State University
Baton Rouge, LA 70803-6417

May 26, 1995

"This study was funded by the Minerals Management Service, U.S. Department of the Interior, Washington, D.C., under contract Number 14-12-0001-30441."

The views and conclusions contained in this document are those of the authors and should not be interpreted as necessarily representing the official policies or recommendations of the Department of the Interior.

Gas Kick Behavior During Bullheading Operations

Principal Investigator: Adam T. Bourgoyne, Jr.
Associate Researchers: William L. Koederitz
Petroleum Engineering Department
Louisiana State University
Baton Rouge, Louisiana 70803-6417

INTRODUCTION

When well control operations are necessary, circulation methods, such as the *driller's method* and the *wait-and-weight method*, are the most widely used and are generally considered the most safe and efficient. However, these circulation methods are not applicable when a kick is taken while (1) the drillstring or bit is plugged or (2) the bit is off bottom, or (3) the drillstring is out of the hole. Also, these circulation methods are not desirable when (1) the kick fluids would be hazardous at the surface, (2) a high rate or high volume of kick fluids cannot be handled at the surface , or (3) excessive pressures are expected at the surface or at the casing shoe. The bullhead method is an alternative in many of the above situations. In the bullhead technique, the operator forces mud into the well from the surface, intentionally causing a subsurface fracture as shown in Figure 1.2. When successful, all of the influx is forced out into the fracture.

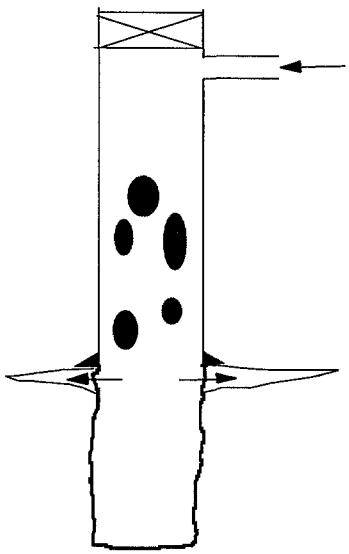

Figure 1.2 Bullhead Method

The bullhead technique is not applicable in all situations since in some instances shallow fractures may reach the surface and cause cratering or may contact fresh water aquifers. In general, these considerations limit the use of the bullhead method to wells with casing set deep enough to prevent shallow fracturing.

Bullheading is currently a trial-and-error technique since a suitable design method is not available. The primary complication in modeling bullheading is the modeling of counter-current flow. While the fluid is pumped downward, the gas has a tendency to flow upward due to the density difference between gas and fluid. Most of the published studies of two-phase flow have focused on co-current flow not counter-current flow. The only papers discussing gas rise velocity are for co-current flow. Johnston (1988) discusses counter-current two-phase flow in pipelines, but this cannot be applied directly to bullheading. No field cases directly applicable to the bullheading well control procedure were found.

A method to predict the efficiency of influx removal and the maximum pumping pressure for a given well situation, kill fluid, and pump rate is desirable. Predicting the volume of kill fluid required and the pumping time are of secondary interest, since the number and the reliability of pumping units and the supply of kill fluid are limiting factors. These secondary interests were not investigated within this study. The primary objectives of this research were (1) to investigate the influx removal efficiency for the bullhead method, (2) to identify the variables of interest, and (3) to develop simple predictive methods. A secondary objective is to develop predictive methods for maximum pump pressure.

EXPERIMENTAL APPARATUS

One of the existing gas storage wells at the LSU Petroleum Engineering Research and Technology Transfer Laboratory was selected for use in this study, since only the surface pipe required modification. A schematic of the gas storage well is shown in Figure 3.1 and the corresponding simulated well design is

shown in Figure 3.2. The well is cased with 7 in., 38 lb/ft casing (inner diameter of 5.92 in., annular capacity of 0.0286 bbl/ft) to a depth of 1,994 ft. A string of 2 3/8 in., 4.7 lb/ft tubing (capacity of 0.00548 bbl/ft) extends to 1,903 ft. Pump input via a 4 in. line enters at the top of the annulus. The tubing output is routed to the SWACO automatic choke through a 4 in. return line. A downhole pressure-sensing tool is suspended on a wireline in the well. Gas is introduced into the annulus of the well via a line at the surface.

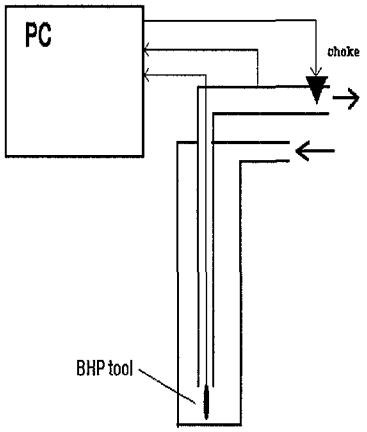

Figure 3.1 Configuration of Research Well

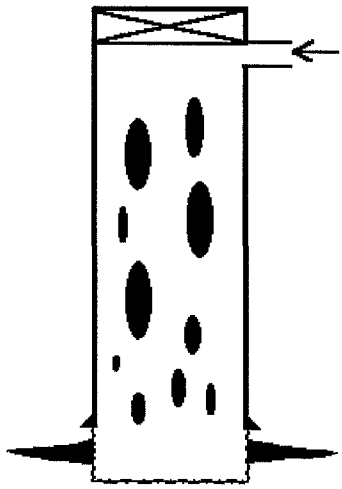

Figure 3.2 Simulated Well Design and Bullhead Situation

An analog/digital data collection and control system directed by a personal computer was installed. The input signals measured were pump pressure, choke manifold pressure, bottomhole pressure, and pump rate. All of the sensors generated 4-20 milliamp current signals, except for the bottomhole pressure sensor which produced an 11-14 KHz signal which was converted to 4-20 milliamps. Two output signals were used for control of the SWACO choke set-point pressure and the mud pump rate. Both of these were 4-20 milliamp control signals.

This combination of wellbore geometry and the computer data collection/control system allowed the tubing string to effectively simulate a subsurface fracture. The computer sensed the bottomhole pressure and the choke manifold pressure in real-time and calculated the optimum choke pressure setting for the desired fracture pressure. This resulted in the "fracture" being closed when bottomhole pressure was below fracture pressure and "opening" (allowing flow out) when bottomhole pressure reached fracture pressure. Since the gas was less dense than the fluids used, once gas and/or liquids from the wellbore entered the tubing string they were permanently removed from the annulus.

A commercially-available choke, the SWACO 10K Kick Killer, was used in this research. This choke's design is based on the "balanced piston" principle, whereby the operator (computer or human) sets a pressure level behind a floating piston which hydraulically balances against the pressure upstream of the choke assembly. This design is more adaptable to computer control, as opposed to choke designs where the operator controls the choke performance by setting an orifice position. In addition to emulating fracture pressure, the fracture logic also needed to position the choke in the optimum position for fastest response such that the choke moved closer to opening as the fracture pressure was approached. The fracture control logic was developed by separately considering the cases of the fracture being open or closed.

CONTROL SYSTEMS LOGIC

When the bottomhole pressure is below fracture pressure (i.e. the fracture is closed), the optimum choke setting is specified by:

$$P_{CKSETP} = P_{CKMAN} + \left(P_{FRAC} - P_{BH}\right) \tag{3.1}$$

This logic keeps the choke closed by the pressure differential of bottomhole pressure below fracture pressure (providing effective sealing performance), and results in the choke being on the verge of opening as fracture pressure is approached (simulating quick fracture action).

The fracture has been defined as a simple model whereby the fracture will open as needed to maintain bottomhole pressure at fracture pressure when the fracture is opened. That is, the fracture will operate (ideally) so as to prevent bottomhole pressure from exceeding fracture pressure. While this is a simple model, it is sufficiently representative for the primary purpose of studying fluid behavior in the annulus during the bullheading process. To meet the bottomhole pressure condition specified, the choke must reduce the bottomhole pressure in the event it exceeds the fracture pressure. This adjustment must also be optimized for efficient and accurate choke positioning. For the case of bottomhole pressure equal to or greater than fracture pressure, the optimum choke setting is specified by:

$$P_{CKSETP} = P_{CKMAN} - \left(P_{BH} - P_{FRAC}\right) \tag{3.2}$$

In the event that the bottomhole pressure exceeded the fracture pressure, this would reduce it by the correct amount, while maintaining flow through the fracture.

Equations 3.1 and 3.2 cover both cases for the fracture, closed and open, and cover all possible bottomhole pressures. Each of these equations is equivalent to:

$$P_{CKSETP} = P_{CKMAN} + P_{FRAC} - P_{BH} \tag{3.3}$$

This results in one direct equation for choke control and does not require knowledge of the fracture state versus time, pressure, or fracture history. An additional benefit of this relationship is that it is computationally efficient and can be used in real-time on current personal computers. Equation 3.3 was used to provide the control logic used for the formation fracture simulator in this research.

To operate the fracture in real-time, the personal computer performed the following tasks in each time step: (1) sensed the bottomhole and choke manifold pressures, (2) calculated the required choke set-point pressure, and (3) set the output current to position the choke at the desired set-point pressure. This control action was done with a direct-control system. A relationship was developed between control current and corresponding choke performance. This relationship was developed directly and dynamically by sending fixed levels of current to the choke and observing the resulting choke manifold pressure once the flow system had reached equilibrium. The pump rates were varied in these experiments, and the resulting relationship between level of control current and choke pressure was linear and independent of pump rate over a wide range of pump rates. This resulted in a direct-control relationship for choke control expressed as follows:

$$I_{CKSETP} = K_0 + K_1 P_{CKSETP} \tag{3.4}$$

Computer control of pump rate had been done before at the LSU research facility for automated well control research. However, the control of the pump rate in this research proved to be more challenging to develop. In comparison with previous research, the pump controller was subject to more severe loading demands on the pump and more rapid changes in pump discharge pressure. For the first attempt, the direct-control approach was tried and quickly proved to be unsatisfactory. Some of the complicating factors that appeared were as follows: (1) time lag between change in control current and pump response, (2) large inertia in pumping system, and (3) interaction between pump rate and pump discharge pressure.

A proportional controller with a feedback loop was developed for the pump control. In each time step, the controller performed the following tasks: (1) sense pump rate, (2) calculate the change in control current based on the needed change in pump rate, and (3) adjust the control current by the calculated change. The equation for the change in control current was as follows:

$$\Delta I_{QP} = \frac{\left(q_{P,TARGET} - q_{P,MEAS}\right)}{K} \tag{3.5}$$

In initial testing, the control factor K was held constant, as is typical for proportional controllers. While this controller performed better than the previous, its performance was not acceptable over the expected range of pump rates and under rapidly-varying discharge pressures. In particular, the controller tended to respond sluggishly when large rate changes were needed and to overshoot when small changes were needed. Further tuning to rectify these two problems was unsuccessful. The control logic was modified so that the constant factor K was replaced by the following function:

$$K = f\left(\left|q_{P,TARGET} - q_{P,MEAS}\right|\right) \tag{3.6}$$

The control program allowed the operator to modify the values and shape of the function for K. Test running the pump at different rates and pressures with linearly-varying functions for K significantly improved pump control performance. However, it was found that due to the inertia of the pump system, it was wise to limit the value of K at extreme changes in pump rate. These observations resulted in the functional shape for K shown in Figure 3.3. The control procedure implemented in the Livewell program provides recommended values for the control function, but allows the operator to change these if needed.

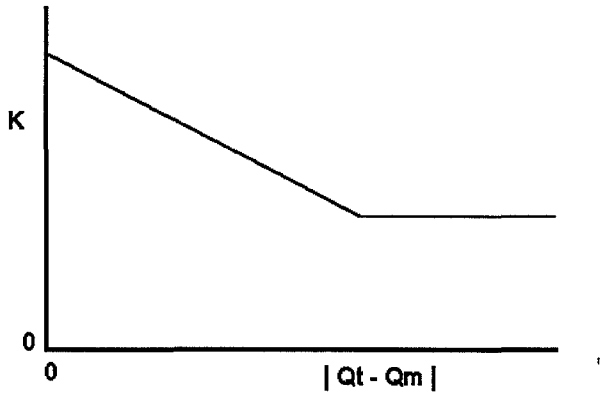

Figure 3.3 Functional Shape of Pump Rate Control "Constant"
(Qt = target pump rate, Qm = meas. pump rate)

EXPERIMENTAL DATA

Prior to injection, the gas was a continuous slug located in the upper-most section of the wellbore. The following variables were considered in this study: (1) fluid properties, (2) fluid injection rates and pressures, (3) fracture gradient, and (4) the initial gas column height and volume. The wellbore geometry and fracture depth were held constant.

A total of twelve experimental runs were completed. Water was used as the bullheading fluid for seven of the runs and a low-viscosity mud was used for the remaining five runs. Table 4.1 shows the properties of the two bullheading fluids used.

Table 4.1 Properties of Bullhead Fluids

Fluid	Density, ppg	Plastic viscosity, cp	Yield Point, lb/100sf
Water	8.34	1	0
Low-vis Mud	8.81	12	7

At the start of each experiment, gas flowed into the annulus directly from a commercial gas pipeline. This flow continued until equilibrium was reached with pipeline pressure and the height of the gas column in the well. The balance between the pipeline pressure and the fluid density resulted in gas column heights of approximately three-fourths of the well depth. Due to variations in gas pipeline pressure with time, there were small differences in initial gas column height and corresponding differences in initial gas volume. To investigate the effect of initial gas column height and volume, one experiment was repeated with an initial gas pressure of one-half of pipeline pressure. This proved to have little effect.

Table 4.3 shows a summary of the experimental runs and the removal efficiencies and all other data derived from these measurements. The experiments covered annular injection velocity ranges from 0.174 to 0.695 ft per sec and formation fracture pressures of 2,000 and 3,000 psi. The removal efficiencies ranged from 0 to 100%.

Table 4.3 Gas Volume Measurements and Injection Velocities

Bull-head Fluid	Frac-ture Press, psi	Pump Rate, gpm	Avg. Annular Velocity, fps	Initial. Gas Press, psi	Initial Gas Height, ft	Initial. Gas Volume, SCF	Final Gas Press, psi	Final BHP, psi	Final Gas Vol, SCF	Rem Eff., %
Water	2,000	12.50	0.174	650	1,572	12,094	*	*	*	0.0*
Water	2,000	25.00	0.347	589	1,404	10,001	498	680	8,123	18.8
Water	2,000	37.50	0.521	644	1,466	11,502	381	716	4,552	60.4
Water	2,000	50.00	0.695	644	1,613	12,659	109	734	422	96.7
Water	2,000	37.50	0.521	320	740	2,710	172	743	923	65.9
Water	3,000	37.50	0.521	627	1,445	10,944	483	770	6,292	42.5
Water	3,000	50.00	0.695	690	1,616	13,716	1158	1930	300	97.8
Mud	2,000	12.50	0.174	607	1,324	9,692	517	779	7,544	22.2
Mud	2,000	18.75	0.260	596	1248	8,953	380	777	4,098	54.2
Mud	2,000	25.00	0.347	616	1337	10,007	109	770	419	95.8
Mud	3,000	12.50	0.174	625	1,344	10,126	462	725	6,624	34.6
Mud	3,000	25.00	0.347	603	1315	9,568	116	867	146	98.5

* indicates computer failure

A short-hand nomenclature was used to identify the experimental runs for use on plots. Each run was identified by bullhead fluid, fracture pressure and, optionally, gas column height. For example, the first experiment was identified as "water, 2000 frac". Figure 4.1 shows the removal efficiencies for the experiments as a function of injection rate.

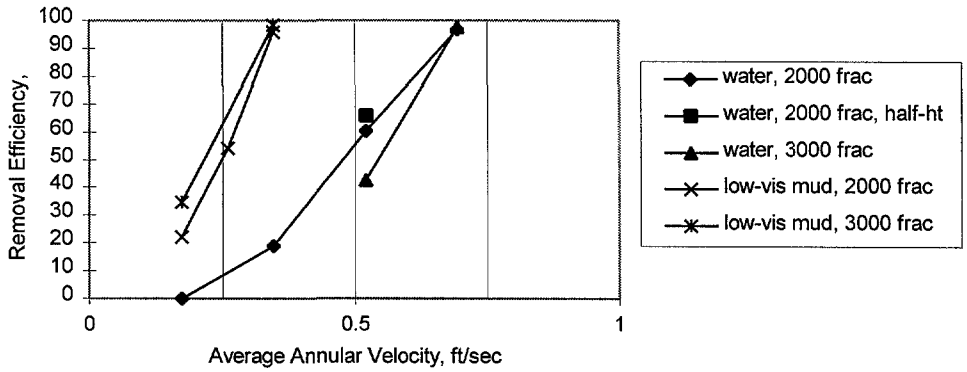

Figure 4.1 Removal Efficiencies as Function of Injection Rate

Notice that the gas is removed completely from the well for injection rates of 1 ft/sec in all cases. With the test mud in the hole, a removal efficiency of 1.0 can still be achieved with an injection rate less than half that of water.

Figure 4.2 shows the typical pressure traverse during an experimental run. The bottomhole pressure, pump pressure and choke manifold pressure gradually increase until the fracture opens. Thereafter, the bottomhole pressure remains constant, within the capability of the controller. The pump pressure plot is horizontal when there is minimal gas removal. When significant amounts of gas are removed from the annulus, the pump pressure decreases. The choke manifold pressure decreases when gas is removed from the well. Using water tends to remove the gas in a more continuous bubble-type flow, whereas the use of mud tends to create slugs of gas. High injection rates also tend to create slug flow.

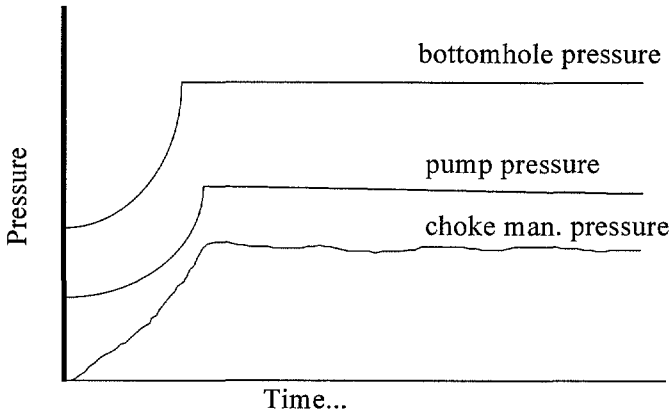

Figure 4.2 Typical Pressure Profiles During Experiments

The displacement efficiency of the bullhead fluid can also be described in terms of Reynolds Number. In this method, it is assumed that the mud completely displaces the annulus. Using a value of 2,000 to 2,200 for the transition from laminar to turbulent flow regimes, it is apparent that all of the mud experiments are in laminar flow, while all of the water experiments are in turbulent flow.

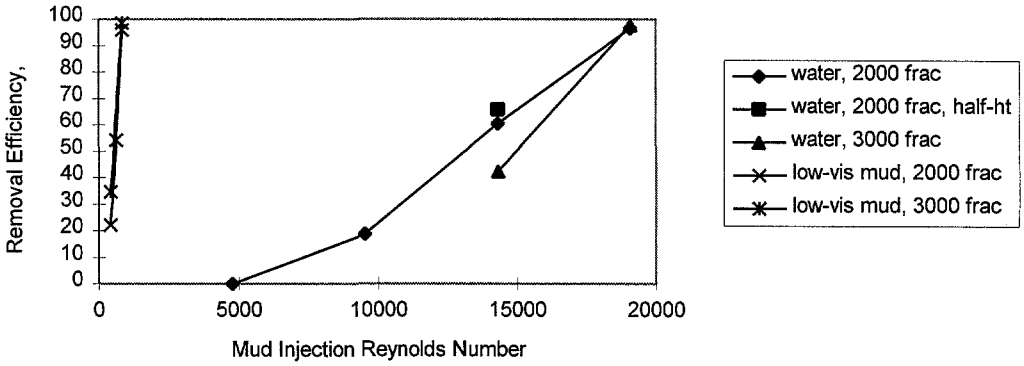

Figure 4.3 Injection Fluid Reynolds Numbers Versus Removal Efficiencies

In two-phase flow, it is common to analyze the flow behavior of the phases in terms of relative velocity, liquid holdup and similar parameters. In this experimental setup it was not possible to measure the required data at any time when the system was in a steady state. However, it is possible to describe the contents of the annulus at the time fracturing starts by considering the following. At the start of the experiment, the annulus contains a known volume of gas in a known space. The rest of the annulus and the tubing is filled with liquid. If the liquid is assumed to be incompressible and the choke is closed prior to fracture, then all injected fluid must go into the original space occupied by the gas. During this process, the gas is compressed as the pressure rises. The location of the gas in this space may vary from all gas on

top (liquid bypasses gas), all gas on bottom (no liquid bypasses gas), or some condition in between. This in-between condition is a mixture of gas and liquid. A variety of methods have been used to describe the condition of this annular space at the time of fracture and to describe the traverse from the start of the experiment to first fracture. The measured factors of interest at the start of fracturing include elapsed time, pump pressure, and injected volume. From these factors, we can derive the slopes for pump pressure change during this initial injection period, in terms of pressure change per unit volume injected and pressure change per unit of time. The measured and calculated values are shown in Table 4.5.

It was observed in the experiments that the maximum pump pressure in all cases occurred at the time the fracture first opened. The pump pressure shown in Table 4.5 at start of fracturing is also the maximum pump pressure during the experiment.

Table 4.5 Experimental Conditions at Start of Fracture

	Frac P, psi	Pump Rate, gpm	Pump P at Start, psi	Pump P at First Frac, psi	Time to Frac, sec	Vol. Injected to Frac, bbl	Slope to Frac, psi/bbl	Slope to Frac, psi/min	Rem. Eff., %
Water	2,000	12.50	653	1423	7273	36.08	21.34	6.35	0.0
Water	2,000	25.00	589	1369	3052	30.28	25.76	15.33	18.8
Water	2,000	37.50	644	1468	2216	32.98	24.99	22.31	60.4
Water	2,000	50.00	644	1468	1840	36.51	22.57	26.87	96.7
Water	2,000	37.50	*	*	1380	20.54	*	*	65.9
Water	3,000	37.50	627	2465	2695	40.10	45.83	40.92	42.5
Water	3,000	50.00	690	2390	2130	42.26	40.04	47.66	97.8
Mud	2,000	12.50	607	1414	5974	29.63	27.54	8.20	22.2
Mud	2,000	18.75	596	1423	3571	26.57	31.05	13.86	54.2
Mud	2,000	25.00	*	*	2760	27.38	*	*	95.8
Mud	3,000	12.50	625	2327	6240	30.95	54.99	16.37	34.6
Mud	3,000	25.00	603	2094	3422	33.95	43.92	26.14	98.5

* indicates computer failure

RESULTS

The experimental data was analyzed and modeled by two different techniques. The goal of both approaches was to develop a method to explain and/or predict the removal efficiency and maximum anticipated pump pressure for the experimental conditions. The first technique used was a theoretical model based on two-phase flow conditions at the time of fracture initiation. The second technique was based on linear statistical modeling techniques using the primary experimental factors as predictors.

THEORETICAL TWO-PHASE FLOW ANALYSIS

The theoretical two-phase analysis can be done if liquid holdup (the fraction of liquid in the two-phase flow area) can be independently determined. Figure 5.1 shows the sequence of annular flow conditions that occur from start of injection until fracturing occurs.

At the start, all gas is in a continuous column at the top of the annulus and has an interface with the mud below. As bullheading fluid is injected into the top of the annulus, it mixes with the gas. Due to the incompressibility of the liquid below, the gas-mud interface does not move. As more liquid is injected, it continues to mix with the gas as the gas is compressed. When the bottomhole pressure has increased to fracture pressure, the fracture opens. The gas-mud interface now moves down as fluid exits the fracture.

A new interface may form on top of the gas-mud mixture such that the injected fluid is now displacing the gas-mud mixture downward. The analysis which follows is based on the assumption that the gas-mud mixture behaves as a continuous two-phase region, and investigates predicted gas velocity with observed removal efficiencies from the experimental runs.

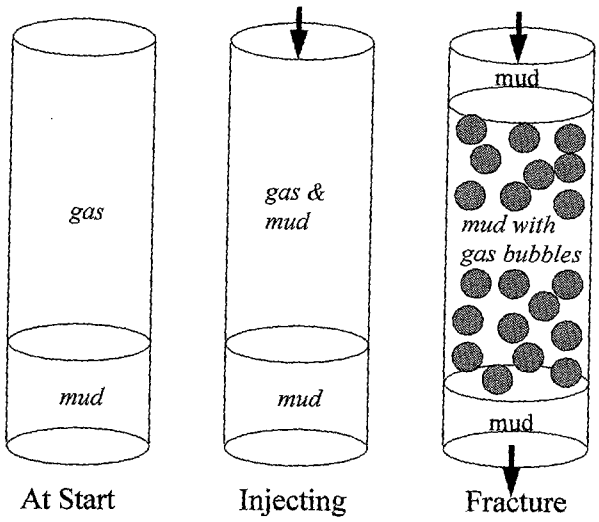

Figure 5.1 Sequence of Annular Flow States From Start to Fracture

At the time fracture occurs, the original gas volume and all of the fluid injected to that time are stored in the physical volume originally occupied by the gas alone. The average liquid holdup for the gas-liquid mixture region can be determined by:

$$H_L = \frac{V_L}{V_{ANN}} \tag{5.1}$$

The calculated values for liquid holdup for the experimental runs are shown in Table 5.1 and are plotted on Figure 5.2. The values range from 69 to 97% over the range of experimental data.

Table 5.1 Calculation of Liquid Holdup at Start of Fracture

Fluid	Frac P, psi	Pump Rate, gpm	Pump P at Start, psi	Initial Gas Volume, bbl	Vol. Injected to Frac, bbl	Average Liquid Holdup, Fraction	Rem. Eff., %
Water	2,000	12.50	650	43.59	36.08	0.828	0.0
Water	2,000	25.00	589	41.33	30.28	0.733	18.8
Water	2,000	37.50	644	41.93	32.98	0.787	60.4
Water	2,000	50.00	644	46.13	36.51	0.791	96.7
Water	2,000	37.50	320	21.16	20.54	0.970	65.9
Water	3,000	37.50	627	41.33	40.10	0.970	42.5
Water	3,000	50.00	690	46.22	42.26	0.914	97.8
Mud	2,000	12.50	607	37.87	29.63	0.783	22.2
Mud	2,000	18.75	596	36.69	26.57	0.724	54.2
Mud	2,000	25.00	616	39.55	27.38	0.692	95.8
Mud	3,000	12.50	625	38.44	30.95	0.805	34.6
Mud	3,000	25.00	603	38.67	33.95	0.878	98.5

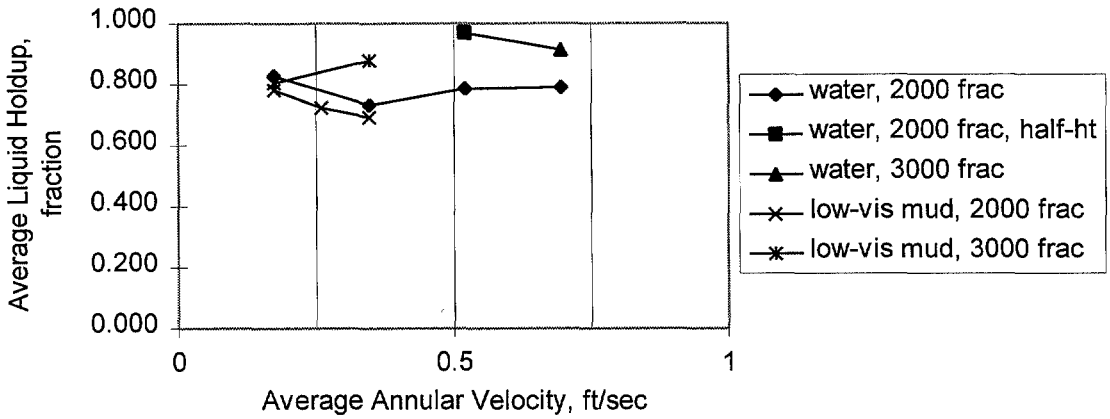

Figure 5.2 Average Liquid Holdup at Start of Fracture

Considering the gas-liquid mixture zone as one region with average properties, the velocity flux across the top interface is equal to that over the lower interface. Gas and liquid velocities are defined as positive in the downward direction. The total flux at the top is equal to the average injection fluid velocity which is also equal to the average mixture velocity. Using actual velocities and average holdup results in:

$$v_{MIX} = v_L H_L + v_G (1 - H_L) \tag{5.2}$$

The bubble rise velocity, v_0, is the velocity difference between the gas and liquid phases. Since all velocities were defined as positive in the downward direction, this is expressed as:

$$v_0 = v_L - v_G \tag{5.3}$$

Combining equations 5.2 and 5.3 and eliminating v_G results in:

$$v_L = v_{MIX} + (1 - H_L) v_0 \tag{5.4}$$

It is assumed that bubble flow is occurring in the annulus, due to the high (69 to 97%) liquid holdups (Griffith and Snyder, 1964). Since slug flow can also exist at bubble flow conditions, the test of Taitel, Barnea and Dukler (1980) (Eqn. 2.13) was used to confirm that slug flow did not exist. The test was done using the conditions most conducive to slug flow (minimum gas density) that occurred in the experimental data. The inequality test result was "5.96>0.79"; confirming the occurrence of bubble flow by the truth of this comparison and the relative values. The velocity difference between the gas and liquid phases for bubble flow can be estimated by the Harmathy equation:

$$v_0 = 1.53 \left(981 \frac{\rho_L - \rho_G}{\rho^2} (70)(8.33) \right)^{0.25} (0.03281) \tag{5.5}$$

Since the average liquid holdups have been estimated, the following procedure can be used to obtain the velocities of both phases for each experiment:

1. For gas, calculate average pressure, z-factor and density.
2. Calculate bubble rise velocity using equation 5.5.
3. Calculate liquid velocity using equation 5.4.
4. Calculate gas velocity using equation 5.3.

The calculations are shown in Table 5.2. Since the pump pressure at fracture is needed to estimate gas density, it is not possible to use the data from the two experimental runs that experienced computer failure and loss of data. These runs are denoted by "*" in Table 5.2.

Table 5.2 Calculation of Liquid and Gas Velocities at Start of Fracture

Fluid	Frac P, psi	Pump Rate, gpm	Avg. Gas P at Frac, psi	Avg. z Factor at First Frac	Gas Density at First Frac, ppg	Average Liquid Holdup, Fraction	Liquid Vel., ft/sec	Gas Vel., ft/sec
Water	2,000	12.50	1712	0.82	0.80	0.828	0.310	-0.482
Water	2,000	25.00	1685	0.82	0.79	0.733	0.559	-0.234
Water	2,000	37.50	1734	0.82	0.81	0.787	0.690	-0.102
Water	2,000	50.00	1734	0.82	0.81	0.791	0.860	0.068
Water	2,000	37.50	*	*	*	0.970	*	*
Water	3,000	37.50	2733	0.81	1.29	0.970	0.544	-0.235
Water	3,000	50.00	2695	0.81	1.27	0.914	0.762	-0.018
Mud	2,000	12.50	1707	0.82	0.80	0.783	0.344	-0.438
Mud	2,000	18.75	1712	0.82	0.80	0.724	0.476	-0.307
Mud	2,000	25.00	*	*	*	0.692	*	*
Mud	3,000	12.50	2664	0.81	1.26	0.805	0.324	-0.447
Mud	3,000	25.00	2547	0.81	1.20	0.878	0.441	-0.331

Figures 5.3 shows the calculated gas velocity as a function of average annular velocity. Inspection of Figure 5.3 shows the gas velocities to be fairly linear with average annular velocity. This is especially true at the lower annular velocities. This applies to gas flow in both directions, downward and upward (a positive velocity was defined to be downward flow). This appears to indicate that the annular flow behavior is similar across the range of the experimental conditions. This is further confirmed by the similarity in liquid holdups. All of these observations are limited to the annular condition at the time fracture first occurs. However, it is postulated in this research that the conditions at the time fracture first occurs significantly affect the displacement processes in the annulus once fracturing starts.

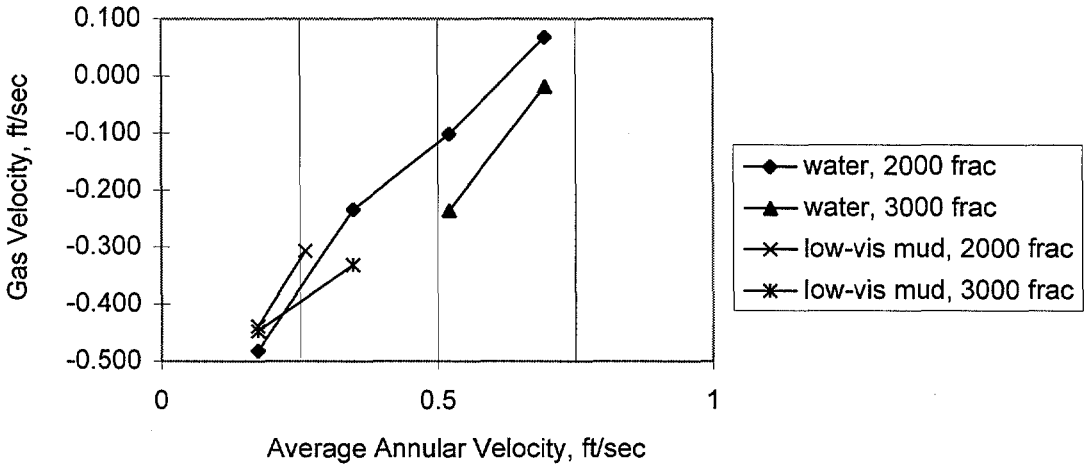

Figure 5.3 Gas Velocities for Experiments

Figure 5.4 shows the removal efficiencies for the experimental runs plotted versus the calculated gas velocities. For all experimental runs, gas velocity is positively correlated with removal efficiency. That is, higher removal efficiencies occurred at higher gas velocities for a given fluid type and fracture pressure. For water, the results are particularly interesting; the complete (or near complete) removal of gas occurred as gas velocities approached positive values. This indicates that the gas as a whole is flowing downward with the bullheading fluid. This is not true for the low-viscosity mud, where high removal efficiencies occurred at lower gas velocities. The low-viscosity mud with 3,000 psi fracture pressure deviates the most from the ideal behavior (high removal efficiency at a calculated upward gas velocity). The "low-vis-mud, 2000 psi frac" case falls in-between the water cases and the "low-vis mud, 3000 psi frac" cases. The primary reason suggested for these differences is that the Harmathy correlation for gas bubble rise velocity is more applicable to water than the viscous drilling mud. Also, the Harmathy correlation is likely more applicable for gas at lower pressures for the low-viscosity mud cases.

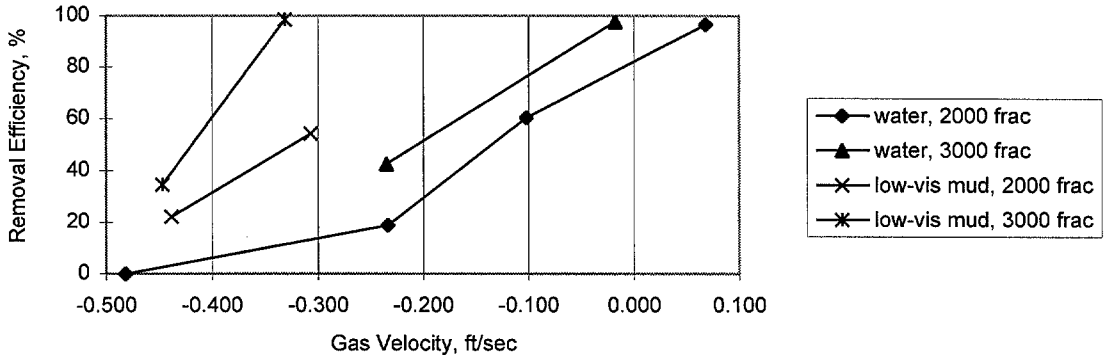

Figure 5.4 Relationship Between Gas Velocity and Removal Efficiency

All of the curves on Figure 5.4 appear to extrapolate to a common negative (i.e. high upward) velocity at near-zero removal efficiencies.

STATISTICAL ANALYSIS OF EXPERIMENTAL DATA

Multiple regression analysis was used in an attempt to develop a predictive method for removal efficiency and maximum pump pressure during bullheading operations. A computer program was used to perform the statistical calculations.

The general estimating model for multiple linear regression is:

$$Y = b_0 + b_1 X_1 + b_2 X_2 + \ldots + b_n X_n \qquad (5.6)$$

where:

Y	=	estimated value of dependent variable,
b_0	=	estimated value for intercept,
b_i	=	estimate for coefficient for X_i,
X_i	=	value of dependent variable i.

Based on the observations made in the Experimental Data section and in the Theoretical Two-Phase Flow Analysis portion of the Results section, nine variables were selected for statistical review. These variables are shown in Table 5.3 along with the short-hand names used for convenience in the analysis and simple descriptive statistics.

The dependent variables of interest are removal efficiency and maximum pump pressure. The primary parameters characterizing each experimental run are fluid used, fracture pressure, and injection rate. Two fluids were used, water and a low-viscosity mud; their properties are described in the Experimental Data section. These fluids were described by an indicator variable, with values of zero for water and one for the mud. The indicator variable was used instead of the actual fluid properties because there were only two fluids used. Use of the fluid properties would add three variables (density, plastic viscosity, yield point) to the model, all correlated to fluid type.

Table 5.3 Experimental Variables Used in Statistical Analysis

Variable	Name	Count	Mean	Standard Deviation
Removal Efficiency, %	RE	12	52.6	35.6
Max. Pump Pressure, psi	PPFRAC	10	1784	470
Injection Fluid	FL	12	N/A	N/A
Fracture Pressure, psi	FRAC	12	2400	516
Injection Velocity, fps	IVEL	12	0.391	0.206
Gas Column Height, ft	HTGAS	12	1441	117
Reynolds Number	NREY	12	8333	7863
Liquid Holdup, fraction	H	12	0.821	0.078
Gas Velocity, fps	VGAS	10	-0.252	0.187

The correlation matrix for the experimental variables chosen is shown in Table 5.4. The removal efficiency is correlated positively with injection velocity. This is apparent from the experimental data. There is no useful information regarding the fluid type (an indicator variable) and fracture pressure since high recoveries were obtained for both fluids. However, the pump pressure at start of fracture is strongly related to fracture pressure only. This strong relationship was the most useful information obtained from the correlation analysis. The other dependent variables are generally unrelated. The few strong relationships that are found are due to interdependencies, particularly with calculated values. This applies to injection velocity, Reynolds Number, holdup and gas velocity. Of these variables, only injection velocity will be used in the following analysis.

Table 5.4 Correlation Matrix for Experimental Variables

	RE	PPFRAC	FL	FRAC	IVEL	HTGAS	NREY	H	VGAS
RE	1.0000	0.3465	-0.0047	0.3813	0.7282	0.3223	0.4438	0.3057	0.7103
PPFRAC		1.0000	0.0556	0.9787	0.2621	0.0704	0.1553	0.8169	0.0485
FL			1.0000	0.1667	-0.6361	-0.8474	-0.8490	-0.2615	-0.5899
FRAC				1.0000	0.1818	-0.0143	0.0353	0.7762	-0.0241
IVEL					1.0000	0.7467	0.9321	0.4044	0.9600
HTGAS						1.0000	0.8659	0.3318	0.6951
NREY							1.0000	0.3586	0.8923
H								1.0000	-0.2615
VGAS									1.0000

The first regression relationship tried was removal efficiency as a function of fluid type, fracture pressure, and injection velocity. An R^2 value of 0.8728 was obtained, with the following equation:

$$RE = -108.1 + 59.13 * FL - 0.00285 * FRAC + 221.8 * IVEL \qquad (5.7)$$

This shows an increase in removal efficiency with mud (over water) and with increased injection velocity, and shows a slight decrease at higher fracture pressure.

The next relationship tested was to predict maximum pump pressure. In the first attempt, all three key variables (fluid type, fracture pressure and injection velocity) were included. This produced the following equation:

PPFRAC = -278.0 - 87.79 * FL + 0.9027 * FRAC + 47.35 * IVEL(5.8)

This equation had an R^2 value of 0.9699. While this was a strong predictor for the data, 99.7% of the model's sum-of-squares was contributed by the FRAC term. In addition, the experimental data and the high correlation coefficient indicate a strong relationship between maximum pump pressure and fracture pressure.

Accordingly, the prediction of maximum pump pressure from fracture pressure only was investigated next. The following relationship resulted:

PPFRAC = -355.5 + 0.8915 * FRAC (5.9)

This resulted in a very slight drop in R^2 (from 0.9699 to 0.9578) and a more robust model. Applying this equation to the experimental data yielded the following predictions:

Table 5.5 Maximum Pump Pressure Predictions from Equation 5.9

Fluid	Frac P, psi	Pump Rate, gpm	Measured Maximum Pump Pressure, psi	Estimate of Maximum Pump Pressure, psi	Residual, psi
Water	2,000	12.50	1423	1427	-4
Water	2,000	25.00	1369	1427	-58
Water	2,000	37.50	1468	1427	41
Water	2,000	50.00	1468	1427	41
Water	2,000	37.50	*	1427	*
Water	3,000	37.50	2465	2319	146
Water	3,000	50.00	2390	2319	71
Mud	2,000	12.50	1414	1427	13
Mud	2,000	18.75	1423	1427	-4
Mud	2,000	25.00	*	1427	*
Mud	3,000	12.50	2327	2319	8
Mud	3,000	25.00	2094	2319	-225

* indicates computer failure

Of the ten estimated values, all but two are within 75 psi of the measured value. The most extreme error, -225 psi, occurs for the "mud, 3000 psi frac, 25 gpm injection rate". This appears to be an anomaly; however, due to the small quantity of data, it will be included in the analysis until further data is collected.

Given the ability to predict pump pressure at the start of fracturing and indications that the annular condition at that time may affect the removal efficiency, a new model for predicting removal efficiency was tried. The following changes were made, compared to the previous regression model for removal efficiency:

1. The estimated maximum pump pressures, using Equation 5.9, were added to the list of independent variables.

2. The "water, 2000psi frac, 12.5gpm" case was removed from the dataset. This was based on the observation that the "true" injection rate for zero removal is above this rate, making this an artificial point that distorts an apparently linear relationship.
3. An auto-correlating regression analysis was used, investigating all combinations of the four dependent variables (fluid type, fracture pressure, injection rate, estimated maximum pump pressure) to find the best model.

This "best fit" model found contained only two of the dependent variables (fluid type, injection rate). The following is the resulting model:

$$RE = -161.4 + 75.9 * FL + 271.3 * IVEL \quad (5.10)$$

This equation had an R^2 of 0.8872 and produced the predictions shown in Table 5.6.

Table 5.6 Removal Efficiency Predictions from Equation 5.10

Fluid	Frac P, psi	Pump Rate, gpm	Measured Removal Efficiency, %	Estimate of Removal Efficiency, %	Residual, %
Water	2,000	12.50	N/A	N/A	N/A
Water	2,000	25.00	18.8	8.6	10.2
Water	2,000	37.50	60.4	55.8	4.6
Water	2,000	50.00	96.7	103.0	-6.3
Water	2,000	37.50	65.9	55.8	10.1
Water	3,000	37.50	42.5	55.8	-13.3
Water	3,000	50.00	97.8	103.0	-5.2
Mud	2,000	12.50	22.2	37.6	-15.4
Mud	2,000	18.75	54.2	61.0	6.8
Mud	2,000	25.00	95.8	84.6	11.2
Mud	3,000	12.50	34.6	37.6	-3.0
Mud	3,000	25.00	98.5	84.6	13.9

As a check on the auto-correlation procedure, independent variables were manually added to and removed from the model; these did not result in improved models. For example, adding fracture pressure to the model increased R^2 from 0.8872 to 0.8897. This model also showed a 7% chance that the coefficient for fracture pressure was zero. Although the model in Equation 5.10 appears to be simple and omits an important variable, Equation 5.10 is the best predictive model based on the experimental data.

Equations 5.9 and 5.10 provide the best estimating technique for this set of experimental data. It is expected that they will provide a basis for improved estimating methods upon further collection of data. Upon collection of more data, it is felt that the use of predictive techniques for the wellbore conditions at the start of fracture, such as maximum pump pressure, liquid holdup and gas velocity, will result in improved models for removal efficiency.

While the two-phase flow approach did not result in promising predictive models for this set of data, the analysis did lend credence to the annular behavior at the start of fracturing. It also showed some correlation between estimated gas velocities and removal efficiencies. While all of these correlations were positive, the cases with water as the bullhead fluid were the most convincing. Upon collection of more data, the two-phase flow approach should be re-tested.

CONCLUSIONS

1. Based on the experimental data, the removal efficiencies for bullheading appear to increase linearly with increasing injection rate, irrespective of the other variables tested. Complete removal of the gas is guaranteed for all cases if the injection rate is greater than 1 ft/sec.

2. The predictive model for maximum pump pressure used formation fracture pressure as the dependent variable. Fluid type and injection velocity were not significant factors in this model. The predictive model for removal efficiency used fluid type (water or mud) and injection velocity as dependent variables. Fracture pressure was not a significant factor in the model. The statistical and theoretical analysis of both models indicates that their use should be limited to the range of the data collected in this experiment. The models would be significantly improved by additional experimental data.

REFERENCES

Davies, R. M., Taylor, G. I., 1950. The Mechanics of Large Bubbles Rising through Extended Liquids and through Liquids in Tubes. Proc. Royal Society, A200: 375-390.

Gillespie, J. F., Morgan, R. F., Perkins, T. K., 1990. Study of the Potential for an Off-Bottom Dynamic Kill of a Gas Well Having an Underground Blowout. SPE Drilling Engineering, Sept. 1990: 215-219.

Griffith, P., Snyder, G. A., 1964. The Bubbly-Slug Transition in a High-Velocity Two-Phase Flow. MIT Rep. 5003-29 (TID-20947).

Harmathy, T. Z., June 1960. Velocity of Large Drops and Bubbles in Media of Infinite or Restricted Extent. A. I. Ch. E. Journal, 6: 281-288.

Johnson, A. B., White, D. B., 1990. Gas Rise Velocities During Kicks. 65th Annual Technical Conference and Exhibition of the Society of Petroleum Engineers, New Orleans, La., Sept. 1990: 295-304.

Johnston, A. J. 1988. An Investigation Into Stratified Co- and Countercurrent Two-Phase Flows. SPE Production Engineering, August 1988: 393-399.

Johnston, A. J. 1988. Controlling Effects in Countercurrent Two-Phase Flow. SPE Production Engineering, August 1988: 400-404.

Nakagawa, E. Y., Bourgoyne Jr., A. T., 1989. Experimentally Determined Gas Slip Velocities in an Inclined Annulus. Proceedings of the International Well Control Symposium, LSU, Baton Rouge, La.

Rader, D. W., Bourgoyne Jr., A. T., Ward, R. H., May 1975. Factors Affecting Bubble Rise Velocity of Gas Kicks. Journal of Petroleum Technology, 571-584.

Taitel, Y., Barnea, D., 1983. Counter-Current Gas-Liquid Vertical Flow, Model for Flow Pattern and Pressure Drop. International Journal of Multiphase Flow, Vol. 9, No. 6: 637-647.

Taitel, Y., Barnea, D., Dukler, A. E., 1980. Modeling Flow Pattern Transition for Steady Upward Gas-Liquid Flow in Vertical Tubes. AIChE J. 26: 345-354.

Taitel, Y., Barnea, D., Dukler, A. E., 1982. A Film Model for the Prediction of Flooding and Flow Reversal for Gas-Liquid Flow in the Vertical Tubes. Int. J. Multiphase Flow 8: 1-10.

Wallis, G. B., 1969. One Dimensional Two-Phase Flow, McGraw-Hill, New York.

Zuber, N., Hench, J., 1962. Steady-State and Transient Void Fraction of Bubbling Systems and Their Operating Limits. Technical Report 62GL100, General Electric Company.